

# Modelling Airway Geometry as Stock Market Data using Bayesian Changepoint Detection

Kin Quan<sup>1</sup>(✉), Ryutaro Tanno<sup>1</sup>, Michael Duong<sup>2</sup>,  
Arjun Nair<sup>3</sup>, Rebecca Shipley<sup>4</sup>, Mark Jones<sup>5</sup>, Christopher Brereton<sup>5</sup>,  
John Hurst<sup>6</sup>, David Hawkes<sup>1</sup>, and Joseph Jacob<sup>1</sup>

<sup>1</sup> Centre for Medical Image Computing, University College London, UK  
kin.quan.10@ucl.ac.uk

<sup>2</sup> Statistical Science, University College London, UK

<sup>3</sup> Department of Radiology, University College Hospital, UK

<sup>4</sup> Mechanical Engineering, University College London, UK

<sup>5</sup> NIHR Biomedical Research Centre, University of Southampton, UK

<sup>6</sup> UCL Respiratory, University College London, UK

**Abstract.** Numerous lung diseases, such as idiopathic pulmonary fibrosis (IPF), exhibit dilation of the airways. Accurate measurement of dilatation enables assessment of the progression of disease. Unfortunately the combination of image noise and airway bifurcations causes high variability in the profiles of cross-sectional areas, rendering the identification of affected regions very difficult. Here we introduce a noise-robust method for automatically detecting the location of progressive airway dilatation given two profiles of the same airway acquired at different time points. We propose a probabilistic model of abrupt relative variations between profiles and perform inference via Reversible Jump Markov Chain Monte Carlo sampling. We demonstrate the efficacy of the proposed method on two datasets; (i) images of healthy airways with simulated dilatation; (ii) pairs of real images of IPF-affected airways acquired at 1 year intervals. Our model is able to detect the starting location of airway dilatation with an accuracy of 2.5mm on simulated data. The experiments on the IPF dataset display reasonable agreement with radiologists. We can compute a relative change in airway volume that may be useful for quantifying IPF disease progression.

## 1 Introduction

Monitoring the progression of airway dilatation in chest CT scans have proven effective as predictors of outcome in idiopathic pulmonary fibrosis (IPF). However, analysis of CT airway images are restricted to crude visual inspection and categorical scores [8]. Computerised quantification of

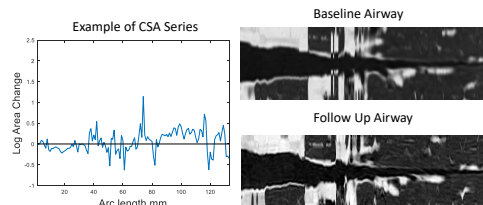


**Fig. 1.** Example of a healthy contiguous CSA change (left) along an airway track between longitudinal scans (right).

change in airway dilatation is limited to computing the difference in cross-sectional area (CSA) on a signal point at each generational branch [9]. Introducing contiguous CSA changes along the airway track (e.g. in Fig. 1) would enable analysis of subtle dilatation. However one would have to distinguish a dilatation from various sources of noise including: (i) Biases and precision from computing CSA such as from centreline generation [13] and lumen identification [6]. (ii) Artefactual measurements such as in bifurcation regions [15]. (iii) Normal biological variations [2].

We introduce a novel application of Bayesian Changepoint Detection (BCPD) for airway quantification in CT. Specifically, to automatically identify the location of airway dilatation of the same airway across longitudinal CT scans in the presence of measurement noise. The BCPD model, typically used in stock market data analysis [12], aims to capture abrupt variations in the underlying distributions of a given signal or a time series. Our method processes a series of CSA changes between baseline and follow-up CT scans, and generates the posterior distribution over multiple possible points of abnormal variations, whose mode is taken as the final prediction. The hypothesis being the initial perturbation of an airway track that can lead to a cascade of events that pushes the overall measure beyond the normal statistical fluctuations seen in a stable system. BCPD models the 1D signals as a distribution of points thus taking account normal biological functions and measurement error. Furthermore, we set the sampling algorithm to choose the number of changepoints thus taking account spurious measurements along the 1D signal. We test the efficacy of the method on (1) CT images of healthy airways with simulated dilatation, and (2) pairs of real images of IPF-affected airways acquired after approximately 1 year. For the simulated datasets, we measured the detection accuracy with respect to the commonly used threshold and maximum likelihood based methods [10]. For the longitudinal IPF dataset we compare the predictions of our model to radiologist interpretation based on two different protocols.

## 2 Method

First we construct a 1D signal of CSA change across longitudinal scans (Sec. 2.1). Secondly, we propose a Bayesian Changepoint model to find locations of abrupt airway dilatation (Sec. 2.2 and 2.3). Finally, we determine the point  $t$  of dilatation (Sec. 2.4).

### 2.1 Airway Pre-processing

For each airway track, we compute a series of CSA measurements [15]. Following interactive identification of the airway, the method outputs a 1D function of CSA along the airway arclength at baseline  $f_B(x)$  and at follow-up  $f_F(x)$  from the carina to the most distal point of the airway (e.g. on Fig. 5). Starting at the carina we resample along the centreline at 1mm intervals using cubic interpolation. We align using the first 50 points on both signals  $g_B, g_F$  and apply the transformation

$f_F(x - a)$  where  $a = \operatorname{argmin}_{a \in [-5, 5]} \left\| \log \left( \frac{g_B(x)}{g_F(x-a)} \right) \right\|_2$ . We consider the series difference defined as  $\mathbf{y} = \log(f_F) - \log(f_B)$  (e.g. of  $\mathbf{y}$  on Fig.1).

## 2.2 Bayesian Changepoint Model

We hypothesise that at the start of dilatation, the series  $\mathbf{y}$  undergoes an abrupt variation, which we refer to as a changepoint. More formally, given signal  $\mathbf{y} = (y_1, \dots, y_n)$  of length  $n$ , we define a changepoint  $\tau$  as the location where there exists a change in parameters  $\theta$  in the underlying distribution  $F$ . In other words, at changepoint  $1 < \tau < n$ , the observations  $\mathbf{y}$  can be separated at  $\tau$  such that  $(y_1, \dots, y_\tau) \sim F(\theta_1)$  and  $(y_{\tau+1}, \dots, y_n) \sim F(\theta_2)$  where  $\theta_1 \neq \theta_2$ . This definition can be naturally extended to the scenario with  $M$  changepoints; we denote the changepoint location vector by  $\tau = (\tau_1, \dots, \tau_k)$ , with parameters  $\theta = (\theta_1, \dots, \theta_{k+1})$  for each respective segment. For ease of notation, we also denote  $\tau_0 = 1$  and  $\tau_{k+1} = n$ . Assuming statistical independence between segments, the likelihood factorises as:  $p(\mathbf{y}|\tau, \theta, M) = \prod_{l=1}^{k+1} F(y_{\tau_{l-1}:\tau_l}|\theta_l)$ , where  $y_{\tau_{l-1}:\tau_l} = (y_{\tau_{l-1}}, \dots, y_{\tau_l})$ . We also specify prior distributions on the number of changepoints  $p(M; \delta)$ , the locations of the changepoints  $p(\tau|M; \gamma)$ , and the parameters of the corresponding segments  $p(\theta|M; \beta)$  where  $\beta$ ,  $\gamma$  and  $\delta$  represent the hyper-parameters.

Given the likelihood and the prior distributions above, we require an estimate of the posterior distribution over the locations of changepoints  $p(\tau|\mathbf{y})$ . As discussed in Sec. 1, our signal  $\mathbf{y}$  is subjected to anatomical and acquisition noise. To overcome these variations in CSA, we choose the likelihood  $F$  as the Student t-distribution [14]. Thus, we denote degrees of freedom  $\nu$ , mean  $\mu$ , variance  $\sigma^2$  and parameter  $\theta = (\mu, \sigma^2, \nu)$ .

## 2.3 Reversible Jump MCMC for Posterior Inference

Posterior inference with our model possesses two challenges. Firstly, without the conjugacy assumption, computing the posterior distribution is intractable. In our case, the Student's t distribution is not an exponential family and therefore cannot have a conjugate prior. Thus the posterior is not available in a closed form. Secondly, the dimensionality of the posterior distribution over the changepoints  $\tau$  is given by  $M$  and varies during inference. To combat the first problem, we use the Metropolis-Hasting (MH) algorithm [1], a variant of Markov Chain Monte Carlo (MCMC) methods that can sample from the posterior, with or without conjugacy. Given that the number of changepoints  $M$  is known, MH can be used to sample from the posterior distributions over the changepoints  $\tau$  and segment parameters  $\theta$ . To address varying posterior dimensionality  $M$ , we extend the above sampling scheme to the Reversible Jump MCMC framework [5]. Taken altogether, the method is capable of traversing the full posterior distributions for  $M, \tau, \theta$  and we refer to this as the Reversible Jump Metropolis Hasting (RJMh) algorithm.

**Overview of RJMH:** The RJMH proceeds by randomly executing one of four possible moves, denoted as  $\Upsilon_i$  at each iteration: (i) resample parameters  $\theta$ ,  $\Upsilon_\theta$ ; (ii) move an existing changepoint,  $\Upsilon_\tau$ ; (iii) add a new changepoint,  $\Upsilon_{M \rightarrow M+1}$ ; (iv) delete an existing changepoint,  $\Upsilon_{M+1 \rightarrow M}$ . We also define the maximum number of changepoints  $k_{max}$  and at the boundary cases for  $k$ , we impose restrictions such that  $\Upsilon_{M \rightarrow M+1}, \Upsilon_{M+1 \rightarrow M}$  are skipped for  $k = 0, k_{max}$  respectively. Each move updates the appropriate subset of parameters  $\theta, \tau$  by sampling from the corresponding distributions  $q(\theta_{new}|\theta_{old})$  and  $q(\tau_{new}|\tau_{old})$ , and is only executed if it passes the associated acceptance criteria  $\alpha$ .

**MH Steps:** For  $\Upsilon_\theta$ , we set  $q(\theta_{new}|\theta_{old}) = (\mu_{old}, \sigma_{old}^2, \nu_{old}) + N(0, \epsilon)$ . This step resamples parameters of each segment by proposing Gaussian perturbations around the current values of parameters for all segments. For  $\Upsilon_\tau$ , we set  $q(\tau_{new}|\tau_{old}) = \tau_{old} + (-1)^b \text{Poi}(\lambda)$  where  $b \sim \text{Binary}[0, 1]$ . This step selects a changepoint  $\tau$  at random and shifts it with a Poisson perturbation. The segments neighbouring this new changepoint location have parameters  $\theta$  resampled as in move  $\Upsilon_\theta$  using the current segment parameters.

**RJ Steps:** For  $\Upsilon_{M \rightarrow M+1}$ , we proposed random new changepoints over our data,  $\tau_{new} \sim U[1, n - 1]$ . The proposed  $\tau_{new}$  split an existing segment into a new left segment  $\theta_l = (\mu_l, \sigma_l^2, \nu_l)$  and new right segment  $\theta_r = (\mu_r, \sigma_r^2, \nu_r)$ . Our proposal for  $\mu_i, \sigma_i^2$  are defined by a Gaussian perturbation on empirical values of the respective  $i = l, r$  segments (Fig. 2). The proposal for  $\nu_i$  is Gaussian perturbation of the previous update  $\nu_{old}$ . Due to dependence of the  $\nu_i$  proposal, a Jacobian term is introduced  $|J_{M \rightarrow M+1}| = 2$ . For  $\Upsilon_{M+1 \rightarrow M}$ , we remove a changepoint  $\tau_{new}$ . As before, proposals for  $\mu_{new}, \sigma_{new}^2$  are defined using empirical values of the segments and Gaussian perturbation (Fig. 2). The proposal for  $\nu_{new}$  is the mean of the previous  $\nu_l, \nu_r$ . The move introduces Jacobian term  $|J_{M+1 \rightarrow M}| = 0.5$ .

**Implementation:** We follow the same RJMH algorithm as defined in the literature [4, 3]. The priors were set as  $\mu \sim N(0, 1)$ ,  $\sigma^2 \sim \text{Scaled-Inv-}\chi^2(5, 0.4^2)$ ,  $\nu \sim U[2, 100]$  and  $M \sim \text{Bin}(n - 1, \frac{0.5}{n-1})$ , where  $\mu, \sigma^2, \nu$  were chosen to be non-informative and within plausible ranges. The expectation for  $M$  was sufficiently low to avoid detecting changepoints in noise. Finally, we set burn-in for 25% of the total iteration count and only storing the 5<sup>th</sup> iteration, after the burn-in period to avoid auto-correlation.

## 2.4 Locating Change in Airway Dilatation

For airways affected by IPF, dilatation starts and progresses from the distal point of the airway [7]. Topologically, we can assume each airway undergoes a

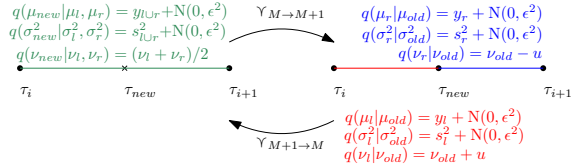


**Fig. 2.** A schematic diagram describing the proposals moves  $\Upsilon_{M \rightarrow M+1}, \Upsilon_{M+1 \rightarrow M}$ . Note that  $u \sim N(0, \epsilon^2)$  and  $y_i, s_i^2$  are the mean and variance respectively of data within the coloured segment.

signal changepoint from which dilatation starts. To locate such a unique changepoint, we consider the posterior over of the changepoint  $p(\tau|\mathbf{y})$ , and perform the following post-processing steps. On each  $\mathbf{y}$ , the proximal region is surrounded by cartilage [16]. The end of cartilage causes an anatomical changepoint independent of disease state. We eliminate it by discounting the most proximal peak on  $p(\tau|\mathbf{y})$ . We then selected the highest peak on the modified posterior  $p(\tau|\mathbf{y})$  as the starting point of dilatation denoted as  $t$ .

### 3 Evaluation & Results

We evaluated our proposed method with two experiments: (i) Simulated dilatations from healthy airways to assess accuracy. (ii) Airways affected by IPF to assess clinical utility. The image properties are displayed on Tab. 1.

Experiment	Patient	BL Voxel Size	FU Voxel Size	Airway	Time between scans
1	1	0.67, 0.67, 1.00	0.56, 0.56, 1.00	6	9M 6D
1	2	0.63, 0.63, 1.00	0.78, 0.78, 1.00	7	35M 6D
1	3	0.72, 0.72, 1.00	0.72, 0.72, 1.00	1	5M 22D
2	4	0.72, 0.72, 1.00	0.64, 0.64, 1.00	3	12M 5D
2	5	0.67, 0.67, 1.00	0.87, 0.87, 1.00	1	10M 24D

**Table 1.** Table of the image properties of voxel size, number of airways used and the time interval between scans. Voxel size is in the form (x,y,z), units: mm. The airways were selected by a trained radiologist R1. All patients in Experiment 1 do not have IPF. Abbreviation: BL - Baseline Scan, FU - Follow-up Scan, M - Months, D - Days.

#### 3.1 Disease Simulation

To quantitatively assess accuracy, a ground truth is required. To this end, we applied our changepoint detection algorithm on augmented healthy airway series to simulate the airway dilatation caused by IPF. A trained radiologist (R1) selected 14 pairs of healthy airways in both baseline and follow-up scans. The image properties are displayed on Tab. 1. They were acquired from different scanners and used different reconstruction kernels. The airways were pre-processed as described in Sec. 2.1 to produce a function of CSA change along the length of the airway.

We modelled the change in dilatation with a logistic function  $l = M/(1 + e^{-\lambda(x-\alpha)})$ , where  $M$  is magnitude of dilatation and  $\alpha$  as the point of dilatation. The parameters  $\alpha$  are set such that the dilatation starts 10-40mm from the distal point and we set  $M$  to range from 0.5-3. Finally we set  $\lambda = 0.5\text{mm}^{-1}$ , in order to create an abnormal increase in CSA. To simulate the dilatation on the airway; the logistic function was added to the logarithmic CSA change of the airways, as shown on Fig. 3. We applied our proposed method to every permutation of  $M$  and  $\alpha$  on each of the 14 healthy airways.

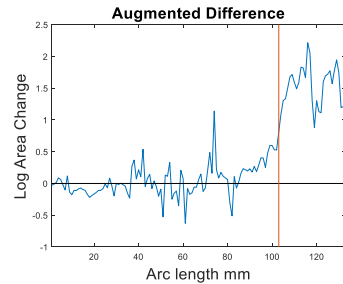


**Fig. 3.** An augmented CSA change from airway on Fig. 1. The red line corresponds to our ground truth as the starting point of dilatation  $\alpha$ .

The proposed method was compared against two conventional methods. First, a basic thresholding method. We smoothed and thresholded the point at which  $\mathbf{y}$  reached above the upper quartile from the right hand side. Secondly, we implemented the method based on Lavielle [10] and implemented in a Matlab inbuilt function; `findchangepts`<sup>7</sup>. In summary we consider  $K$  changepoint and these changepoints  $y_i$ , minimize the function:  $J(K) = \sum_{r=0}^{K-1} \sum_{i=k_r}^{k_{r+1}-1} \Delta(y_i, y_{k_r:k_{r+1}-1}) + \beta K$ , where  $\beta$  is modified such that the function finds less than  $K$  changepoints. We found  $\Delta = y_i - \text{mean}(y_{k_r:k_{r+1}-1})$  gives the most accurate results. The method [10] assumes the data  $\mathbf{y}$  is Gaussian distributed. To replicate the post processing in Sec. 2.4, we consider  $K = 2$  possible changepoints and minimum distance of 20mm. This takes into account the changepoint caused by the support cartilage. The most peripheral point was chosen as the point of dilatation.

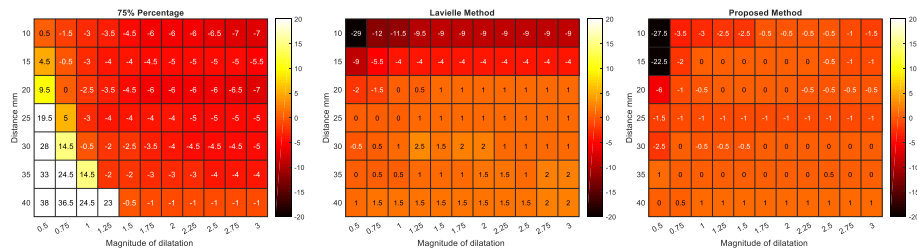


**Fig. 4.** Heatmap showing the accuracy of each method in mm. (Left). Thresholding method. (Middle). Method from Lavielle [10]. (Right). Our proposed method. The colour scale is the same on all of the heatmaps.

Fig. 4 shows the accuracy for each method as a heatmap. Each entry on the heatmap corresponds to the median average of all displacements over 14 airway pairs. A positive displacement corresponds to an overestimation of the ground truth towards the distal point. When the magnitude of dilatation is larger than  $M > 0.75$ , our proposed method achieves consistently higher accuracy than Lavielle [10]. The accuracy gain in the peripheral regions of the airways at  $\alpha = 10\text{-}30\text{mm}$  from the distal point are the most clinically relevant in IPF as parenchymal damage begins in the lung periphery and progresses proximally [7]. Furthermore, on the same peripheral regions  $\alpha = 10\text{-}30\text{mm}$ , the baseline method showed systematic bias in accuracy towards the central airways. This was due to the baseline method being influenced by outliers from the longer expanses of normal airway regions. The proposed method uses the t-distribution as the likelihood thus making it robust to possible outliers within the data [14]. The proposed method suffers from poor accuracy below magnitudes of dilatation  $M = 0.75$ . However, in physical terms a dilatation of  $M = 0.75$  corresponds to a percentage increase in CSA of  $e^{0.75} - 1 \approx 112\%$ . This is within the range of normal change of the airways [2].

<sup>7</sup> <https://www.mathworks.com/help/signal/ref/findchangepts.html> last accessed on August 14, 2019.

### 3.2 Application to Airways affected by IPF

To show clinically utility, we acquired 4 airway pairs from 2 patients (Tab. 1). All airways were judged by the radiologist R1 to be dilated as a consequence of IPF on baseline and to have visually worsened on follow-up imaging.

We compared the performance of our method against two trained thoracic radiologists R1, R2. To assess the reproducibility of manual labelling, each radiologist labelled the same airway twice through two different protocols. First, the radiologists interrogated axial CT images. Using 2 separate workstations and the airway centreline, the radiologists identified the point on the centreline (on the follow-up scan) where the airway demonstrated definitive worsened dilatation. Second, the radiologist compared the aligned reconstructed cross-sectional planes on baseline and follow-up scans (e.g. Fig. 5). The radiologist then selected the slice where the airway had worsened when evaluated against the baseline.

The results (Fig. 5) indicate that the predictions for Airway 1, 3 and 4 are within the range of the radiologists’ labels. In the case of Airway 2 our method overestimates compared to radiologists’ predictions. The posterior distribution contains another equally probable peak that underestimates the radiologists’ labels (see the second highest peak at 70mm), potentially indicating a more proximal point of dilatation. To test this, we delineated the boundary of the lumen on the reconstructed cross sectional slices at baseline in the neighbourhood of this peak, and Fig. 5 shows the initial few slices (62-64mm). When the delineated boundary from baseline was superimposed on the follow-up scan, the boundary is contained inside the follow-up lumen. This result indicates that the starting point of dilatation is more proximal than the labels from the radiologists.

**Volumetric Analysis:** By computing the starting point  $t$  of dilatation of the airways, we can compute airway volume changes in diseased and healthy regions of the airway track by integrating CSA measurements along arclength  $f_F, f_B$ . We used the trapezium rule to find 3 volumetric regions: (i) the entire airway track,  $V_{c \rightarrow d}$ , (ii) carina to  $t$ ,  $V_{c \rightarrow t}$ , (iii)  $t$  to the distal point  $V_{t \rightarrow d}$ . Tab. 2, shows the results of the percentage volume change. The volume change in  $V_{t \rightarrow d}$  had greater sensitivity for selecting progressive airway dilatation in IPF than the volume change in the entire airway  $V_{c \rightarrow d}$ .

Airway	PVC of $V_{c \rightarrow d}$	PVC of $V_{t \rightarrow d}$	PVC of $V_{c \rightarrow t}$
1	2.6 %	32.9%	1.1%
2	3.2 %	129.7%	2.2%
3	2.6 %	47.4 %	-0.3%
4	7.4 %	48.4 %	7.1%

**Table 2.** The percentage volume change (PVC %) for each region of the airway.

## 4 Discussion & Conclusion

In this paper, we propose a novel application of the BCPD in detecting airway dilatation caused by progression of IPF. The model uses a series of CSA changes between longitudinal scans with presence of normal biological variation and precision errors in measuring CSA. Experiments on simulated data show our model can detect the starting location of airway dilatation with superior accuracy to competing methods. The results display reasonable agreement with radiologists. One case indicated a more plausible location of dilatation, potentially missed

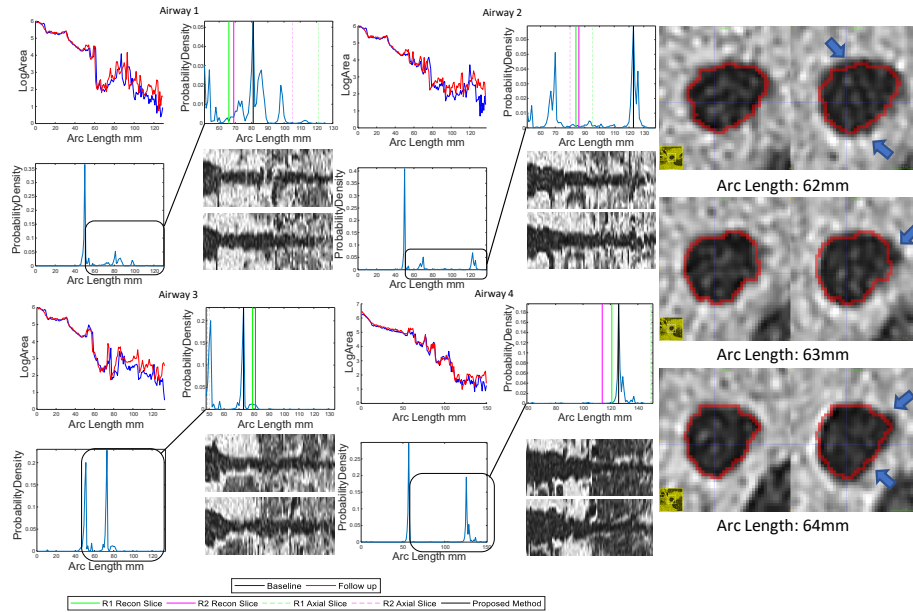


**Fig. 5.** Left: The log CSA and posterior distribution  $p(\tau|\mathbf{y})$  for each of the four airway pairs. In the magnified region (black) we compared the labels from our proposed method with the radiologist. The top and bottom reconstructed airway corresponds to the baseline and follow up scans respectively. Right: A row of three consecutive reconstructed slices in Airway 2, arc length of 62-64mm, baseline (left) and follow-up (right). The boundary delineation (red) from the baseline are superimposed on the follow-up scan. The blue arrows indicate pixels from the lumen outside the boundary.

by the experts. There is a clinical need for head to head comparisons for the effectiveness of drugs in treating IPF [11]. Identifying a change in airway dilatation over time could become a sensitive measure of IPF worsening, providing an important secondary endpoint in drug trials. As future work, we believe the technology can be applied to other progressive diseases that results in a cascade of events leading to spread of pathology, such as the growth of plaque and aneurysms in major blood vessels.

## Acknowledgements

Kin Quan is supported by the EPSRC-funded UCL Centre for Doctoral Training in Medical Imaging (EP/L016478/1) and the Department of Health NIHR-funded Biomedical Research Centre at University College London Hospitals. Ryutaro Tanno is supported by Microsoft Research Scholarship. Micheal Duong is funded by the Centre for Doctoral Training in Financial Computing and Analytics. Arjun Nair is funded by National Institute for Health Research Biomedical Research Centre. Mark Jones & Christopher Brereton are supported by National Institute for Health Research. Joseph Jacob is a recipient of Wellcome Trust Clinical Research Career Development Fellowship 209553/Z/17/Z.



## References

1. S Chib et al. Understanding the Metropolis-Hastings Algorithm. *The American Statistician*, 49(4):327–335, 1995.
2. L Gazourian et al. Quantitative computed tomography assessment of bronchiolitis obliterans syndrome after lung transplantation. *Clinical Transplantation*, 31(5):e12943, 2017.
3. A Gelman et al. *Bayesian Data Analysis*. CRC Press, 2014.
4. P J Green. Reversible jump Markov chain monte carlo computation and Bayesian model determination. *Biometrika*, 82(4):711–732, 1995.
5. P J Green et al. Reversible jump MCMC. *Genetics*, 155(3):1391–1403, 2009.
6. S Gu et al. Computerized identification of airway wall in CT examinations using a 3D active surface evolution approach. *Medical Image Analysis*, 17(3):283–96, 2013.
7. J Jacob et al. HRCT of fibrosing lung disease. *Respirology*, 20(6):859–872, 2015.
8. J Jacob et al. Serial automated quantitative CT analysis in idiopathic pulmonary fibrosis: functional correlations and comparison with changes in visual CT scores. *European Radiology*, 28(3):1318–1327, 2018.
9. P Konietzke et al. Quantitative CT detects changes in airway dimensions and air-trapping after bronchial thermoplasty for severe asthma. *European Journal of Radiology*, 107:33–38, 2018.
10. M Lavielle. Using penalized contrasts for the change-point problem. *Signal Processing*, 85(8):1501–1510, 2005.
11. D Lederer et al. Idiopathic pulmonary fibrosis. *The New England Journal of Medicine*, 378(19):1811–1823, 2018.
12. T Mikosch et al. Changes of structure in financial time series and the GARCH model. *REVSTAT Statistical Journal*, 2(1):41–73, 2004.
13. K Palágyi et al. Quantitative analysis of pulmonary airway tree structures. *Computers in Biology and Medicine*, 36(9):974–96, 2006.
14. S J D Prince. *Computer Vision: Models, Learning, and Inference*. Cambridge University Press, 2012.
15. K Quan et al. Tapering analysis of airways with bronchiectasis. In *Proceedings of SPIE*, 2018.
16. E R Weibel. *Morphometry of the Human Lung*. Springer, 1963.